

# **Gate Tunable Dissipation and Superconductor-Insulator Transition in Carbon Nanotube Josephson Junctions**

Gang Liu, Yong Zhang and Chun Ning Lau\*

Department of Physics and Astronomy, University of California, Riverside, Riverside, CA 91765

\* To whom correspondence should be addressed. [lau@physics.ucr.edu](mailto:lau@physics.ucr.edu)

## **Abstract**

We observe gate-tunable hysteretic voltage current characteristics in single-walled carbon nanotubes coupled to superconductors. The hysteresis size anti-correlates with the normal state conductance, indicating junction dynamics undergoes periodic modulation between underdamped and overdamped regimes. When the Fermi-level of the nanotube is tuned through a local conductance minimum, we observe a gate-dependent transition from superconducting to insulating regimes. Our results underscore the potential of carbon nanotubes as a gate-tunable model of Josephson junctions.

PACS numbers: 73.63.-b, 73.63.Fg, 74.45.+c, 74.50.+r

Dissipation in superconducting systems is ubiquitous, and is intimately associated with the maintenance of superconducting phase coherence. For instance, change in dissipation has been associated with superconductor-insulator transition (SIT) observed in single Josephson junctions (JJ)[1], one-dimensional (1D) superconducting nanowires[2], two-dimensional (2D) JJ arrays[3], and 2D superconducting thin films [4]. In particular, dissipation in single or arrays of JJs has been the focus of much theoretical work[5-10]. With the exception of ref. [3], in which an 2D JJ array was fabricated above a semiconductor heterostructures with tunable resistance, dissipation in these systems are determined by device geometry and/or shunt resistors, and cannot be tuned *in situ*; thus direct tests of theoretical predictions are not straightforward because of inevitable variability in fabricated mesoscopic devices.

Here we report observation of gate tunable dissipation and evidence for dissipation driven SIT in single-walled carbon nanotube (SWNT) Josephson transistors[11-20]. As the device is tuned by gate voltage from resonant to off-resonant transmission across the quantized energy levels, the critical current  $I_c$  decreases significantly, while the voltage-current ( $V$ - $I$ ) characteristics change from non-hysteretic to strongly hysteretic. This suggests that the junction crosses over from overdamped to underdamped regimes, in agreement with estimates from the model of resistively and capacitively shunted junctions (RCSJ). Moreover, as the Fermi level of a device is tuned through a local resistance maximum, we observe a superconductor-insulator transition, characterized by the opposite dependence of zero bias resistance  $R_0$  on temperature  $T$  and bias  $I$ . Our results demonstrate continuous modulation of damping in individual devices, and constitute the first observation of gate tunable SIT in single JJ. Such SWNT JJ will enable *in situ*

study of the interplay between dissipation and quantum coherence, thus offering a capability difficult to achieve in other superconducting systems.

The SWNTs are synthesized by chemical vapor deposition on highly doped Si/SiO<sub>2</sub> substrates[21]. The electrodes are fabricated by standard electron beam lithography, and consist of 5nm of palladium and 80 nm of aluminum(Al) (Fig. 1a inset). Only nanotubes with room temperature resistance below 20k $\Omega$  are measured in a <sup>3</sup>He refrigerator. Similar results were observed in 4 different devices. For a typical device, the normal state linear-response conductance  $G_N$  oscillates sinusoidally as a function of gate voltage  $V_g$  (Fig. 1a). Its magnitude varies between 80 and 125  $\mu$ S, approaching the theoretical limit of  $G_Q=4e^2/h\approx 158 \mu$ S for a perfectly coupled SWNT, indicating highly transparent electrode-nanotube interfaces. Fig. 1b displays non-linear transport spectroscopy measurement of the same device at 260mK, plotting differential conductance ( $dI/dV$ ) as a function of  $V_g$  and applied bias. The striking checker-board pattern is a signature of Fabry-Perot interference of electron waves in the nanotube, whereas the conductance maxima (minima) correspond to the resonant (anti-resonant) transmission of charges via discrete energy levels, which arise from the finite length of the nanotube. The characteristic energy scale of the oscillation  $eV_c$ , indicated by the black dot in Fig. 1b, yields the level spacing  $h\nu_F/2L$ , where  $e$  is the electron's charge,  $h$  is the Planck's constant,  $\nu_F \sim 10^6$  m/s is the Fermi velocity, and  $L$  is the distance traveled by charges between successive scatterings. From Fig. 1b, we obtain  $V_c\approx 11.8$ mV, suggesting  $L\approx 175$  nm. This is in excellent agreement with the measured source-drain spacing of 180 nm, indicating that scattering only occurs at the nanotube-electrode interfaces. Thus, the measured high conductance, together with the clear Fabry-Perot features that extend over a large  $V_g$  range, establish that our SWNT devices are free

of defects, well-coupled to electrodes, and support ballistic and phase coherent transport of charges.

At small biases  $V < 2\Delta$ , the effect of the superconducting electrodes manifests as dramatically enhanced conductance ( $\Delta$  is the superconducting energy gap of Al). As shown by the central bright band in Fig. 1b and the higher resolution image in Fig. 1c (notice the logarithmic conductance scale), the conductance peaks at zero bias reach a few  $\text{mS} \gg G_Q$ , indicating the presence of a supercurrent. At small but finite biases, we observe conductance peaks at sub-harmonic multiples of  $2\Delta$  (Fig. 1c). These peaks, which arise from multiple Andreev reflections (MAR) of charges at the superconductor-SWNT interfaces[11, 22, 23], persist through the gate voltage range, and yield an estimated  $2\Delta \sim 240 \mu\text{eV}$ .

We now focus on the  $V$ - $I$  characteristics of the device in the current bias regime. At small current bias  $I < \sim \text{nA}$ , supercurrent was observed, characterized by a zero or very low voltage; when the bias exceeds a critical value  $I_c$ , the device switches from the supercurrent branch to a resistive branch, with a slope that approaches  $1/G_N$  at high biases. Unlike a standard JJ, where the  $V$ - $I$  curve depends only on temperature, a SWNT JJ displays dramatic variation in  $V$ - $I$  characteristics with  $V_g$ , resulting from the tuning of the electrodes' Fermi levels with respect to the quantized energy levels in the nanotube. Three representative traces at different gate voltages are shown in Fig. 2a, and  $\alpha$ ,  $\beta$  and  $\gamma$  corresponds to on-resonance, intermediate and off-resonance transmission, respectively.

For two superconductors coupled via discrete energy levels with 2 spin-degenerate channels, the critical current in the wide resonance regime, which is appropriate to our devices with extrinsic level widths  $\Gamma > \sim \text{meV}$ , is[24]

$$I_c \approx \frac{2e\Delta}{\hbar} \tanh\left(\frac{\Delta}{2k_B T}\right) \left[1 - \sqrt{1 - \frac{G_N}{4e^2/h}}\right] \quad (1)$$

where the term in the square brackets takes into account of the asymmetric coupling between the SWNT and the two electrodes, and  $k_B$  is Boltzman's constant. Thus Eq. (1) predicts that  $I_c$  increases with increasing  $G_N$ . This is borne out in Fig. 2a: at resonant states with maximum  $G_N$  ( $\gamma$  trace), the measured  $I_c$  is largest, 8.3 nA;  $I_c$  decreases with  $G_N$ , reaching a minimum of 1.1 nA when the transmission is off-resonant ( $\alpha$  trace) (see also Fig. 2b). Here we take the value of  $I_c$  be that of the largest slope  $dV/dI$ .

The dependence of  $I_c$  on gate voltage has been studied in previous experiments [11-20]. A relatively unexplored aspect is the detailed shape of the  $V$ - $I$  curves, which contain a wealth of information on the junction dynamics. For instance, within the RCSJ model, the  $V$ - $I$  characteristic of an underdamped junction in the strong coupling regime ( $E_J \gg k_B T$ ) is hysteretic, displaying sharp switching from supercurrent to resistive branches at  $I_c$ , and the reverse transition from resistive to supercurrent branches occurs at retrapping current  $I_r < I_c$ . Here  $E_J = \frac{\hbar I_c}{2e}$  is the Josephson coupling energy. At finite temperatures, thermal fluctuations reduce  $I_c$  but increase  $I_r$ , thereby reducing the hysteresis size, until  $I_r = I_c$  at  $E_J \sim k_B T$ . In comparison, in an overdamped junction the transition from supercurrent to resistive branches is *always* smooth and non-hysteretic. Thus, hysteresis observed in the  $V$ - $I$  characteristics, or the lack thereof, is an important indication of the junction dynamics, as well as the relative magnitudes of Josephson coupling to thermal fluctuations.

Examining the three  $V$ - $I$  curves in Fig. 2a, we observe that the  $\alpha$  trace, which has the smallest  $I_c$  and corresponds to off-resonance transmission, displays sharp switching in both current directions, with the largest hysteresis. For the  $\beta$  trace, hysteresis is small but observable.

Both curves suggest relatively small dissipation in the junction. In contrast, the  $\gamma$  trace for on-resonance transmission has the largest  $I_c$ ; it is also smooth and entirely non-hysteretic, resembling that of an overdamped junction. Thus, *when the transmission is tuned from on- to off-resonance,  $I_c$  decreases while hysteresis increases*. Similar trend is observed over a large range in  $V_g$ : Fig. 2b displays the measured junction voltage (grayscale) as a function of current bias (vertical axis) and  $V_g$  (horizontal axis) *for both directions of current-sweeping* -- the up-sweep plot is set to be 50% transparent and superimposed on the down-sweep plot. The white and dark areas corresponding to the resistive branches, and light gray areas correspond to the supercurrent branch. The values of  $I_c$  and  $I_r$  can thus be easily determined from the outlines separating the supercurrent regions and the resistive regions.

A quantitative analysis is presented in Fig. 3. The top panel plots the gate dependence of  $I_c$  (circles) and  $I_r$  (filled circles), and the bottom panel plots the ratio  $I_c/I_r$  that parameterizes the size of hysteresis. For ease of comparison, we also plot  $G_N(V_g)$  on the right axis on the bottom panel (dotted line). Clearly, the hysteresis size anti-correlates with  $I_c$  and  $G_N$ . The ratio is  $\sim 1$  when  $G_N \sim 3e^2/h$ , and increases to  $\sim 1.6$  at  $G_N \sim 2e^2/h$ . Naively, we expect that in an underdamped junction, the hysteresis size directly correlates with the ratio  $E_J/kT$ ; hence large hysteresis should occur at on-resonant transmission, which is exactly opposite to what we observed experimentally.

Motivated by the observed anti-correlation of hysteresis and  $G_N$ , we consider the possibility of gate tunable damping in the SWNT JJ. Within the RCSJ model, dissipation can be parametrized by  $1/Q$ , where  $Q$  is the junction's quality factor, given by[25]

$$Q = \omega_p R_j C_j, \quad (2)$$

where  $\omega_p = \sqrt{\frac{2eI_c}{\hbar C_j}}$  is the plasma frequency,  $R_j$  and  $C_j$  are the shunt resistance and capacitance of the junction, respectively. Thus  $Q > 1$  corresponds to underdamped regimes. In the absence of an external shunt resistor,  $R_j \sim R_N$ , and  $C_j$  is estimated from geometric capacitance and gate conversion factor to be  $\sim 0.2\text{fF}$ . For typical  $R_N \sim 10\text{ k}\Omega$ , we obtain  $Q \sim 1.3$ , indicating that the junction is close to critically damped. This is consistent with our observation of transition from underdamped to overdamped regimes, as  $G_N$  is modulated by gate voltage. At  $T=0$ ,  $Q$  is related to the ratio  $I_c/I_r$  by[25]

$$I_c/I_r = \pi Q/4 \quad (3)$$

In the presence of thermal fluctuations, the ratio is expected to decrease; nevertheless, in general  $I_c/I_r$  can serve as a measure of dissipation in the junction at a fixed temperature. Combining Equ. (2) and (3), we obtain  $I_c/I_r \propto Q \propto 1/G_N$ , as observed experimentally (Fig. 3). Thus, our results show that dissipation in the SWNT junction is proportional to normal state conductance, which is continuously tunable by gate voltage.

The observation of gate tunable dissipation raises the possibility of observing superconductor-insulator transition (SIT) in SWNT Josephson junctions: for sufficiently small  $G_N$ , low dissipation may result in delocalization of the phase of the superconducting order parameter, *i.e.*, an insulating phase. Evidence for such a transition was shown in Fig. 4a. The upper inset plots  $G_N$  vs.  $V_g$  for device 2, which exhibits regular Fabry-Perot patterns for  $V_g < 9\text{V}$ ; however, at  $V_g \sim 10.5\text{V}$ , there exists a particularly resistive period with a minimum  $G_N \sim 3\mu\text{S}$ . Such a resistive state may arise from the presence of a small bandgap[26]. Within the gap, the  $V$ - $I$  characteristics is dramatically different from those at other gate voltages:  $R_0 \sim 3\text{M}\Omega \gg R_N$ , and decreases to  $R_N$  for  $V > 2\Delta$  (Fig. 4a, red curve). This resembles that of an insulating junction, and is in stark contrast with the typical  $V$ - $I$  characteristics of a superconducting junction shown in

Fig. 2, in which a small  $R_0$  increases to  $R_N$  at high current biases. Such insulating behavior within the gap is further verified by the temperature dependence of the  $V$ - $I$  characteristics. The main panel of Fig. 4a plots the  $V$ - $I$  curves at  $V_g \sim 10.5$  V at 260 mK, 530 mK and 700 mK, respectively, showing decreasing  $R_0$  with increasing temperature; the larger bias  $V$ - $I$  curves are shown in the lower inset. Note that  $R_N$ , *i.e.*, the slope of an  $V$ - $I$  curve at high biases, stays constant for all three temperatures, indicating that the negative  $R_0$ - $T$  dependence arises entirely from superconductivity. For comparison, the  $V$ - $I$  curves at gate voltages outside the gap are shown in the middle inset, displaying  $R_0$  increases with higher  $T$ .

Further evidence for a gate-tunable SIT is the temperature dependence of  $R_0$  of the junction at a number of gate voltages with different  $R_N$ , as shown in Fig. 4b. The top curve corresponds to that at the center of the gap. At  $T \sim 1$  K, the  $V$ - $I$  characteristics are linear, and  $R_0 = R_N$ . As temperature is decreased, depending on the value of  $R_N$ , a clear divergence of behavior is evident: at gate voltages with  $R_N \sim 10$  k $\Omega$ ,  $R_0$  decreases with temperature and approach 0 at 260 mK; when  $R_N > 20$  k $\Omega$ ,  $R_0$  increases with temperature; those gate voltages with intermediate  $R_N$  have almost constant  $R_0(T)$ . This dichotomy of behavior is clearly visible despite the scattering in the data points, which arises from shifts in the effective gate voltage due to random fluctuation in the charge environment. Thus the junction may be superconductor-like or insulator-like, depending on a “critical” value of  $R_N \sim 8$ -20 k $\Omega$ . Such behavior is reminiscent of the dissipation-driven SIT observed in 2D superconducting thin films and JJ arrays, where the transition occurs when the sheet resistance is equal to  $h/4e^2 \sim 6.5$  k $\Omega$  [1, 3, 27]. In the context of gate tunable dissipation described in the first part of the letter, the SIT is likely driven by modulations in dissipation, though the detailed dynamics and dissipation mechanism warrant further experimental and theoretical investigation.



In conclusion, we observed gate tunable dissipation and superconductor-insulator transition in SWNT Josephson junctions, which continue to offer a unique platform for exploring the interplay between dissipation and quantum coherence.

We thank Leonid Pryadko and Marc Bockrath for helpful discussions. This research is supported in part by NSF CAREER DMR/0748910 and ONR/DMEA Award H94003-07-2-0703.

## References

1. J. S. Penttila *et al.*, Phys. Rev. Lett. **82**, 1004 (1999).
2. A. Bezryadin, C. N. Lau, and M. Tinkham, Nature **404**, 971 (2000).
3. A. J. Rimberg *et al.*, Phys. Rev. Lett. **78**, 2632 (1997).
4. N. Mason and A. Kapitulnik, Phys. Rev. B **65** (2002).
5. C. P. Herrero and A. D. Zaikin, Phys. Rev. B **65**, 104516 (2002).
6. G. Refael *et al.*, Phys. Rev. B **68** (2003).
7. F. K. Wilhelm, G. Schon, and G. T. Zimanyi, Phys. Rev. Lett. **87**, 136802 (2001).
8. L. I. Glazman and A. I. Larkin, Phys. Rev. Lett. **79**, 3736 (1997).
9. S. Chakravarty *et al.*, Phys. Rev. Lett. **56**, 2303 (1986).
10. P. Goswami and S. Chakravarty, Phys. Rev. B **73**, 094516 (2006).
11. M. R. Buitelaar *et al.*, Phys. Rev. Lett. **91**, 057005 (2003).
12. M. R. Buitelaar, T. Nussbaumer, and C. Schonenberger, Phys. Rev. Lett. **89**, 256801 (2002).
13. H. I. Jorgensen *et al.*, Phys. Rev. Lett. **96**, 207003 (2006).
14. P. Jarillo-Herrero, J. A. van Dam, and L. P. Kouwenhoven, Nature **439**, 953 (2006).
15. T. Tsuneta, L. Lechner, and P. J. Hakonen, Phys. Rev. Lett. **98**, 087002 (2007).
16. J. P. Cleuziou *et al.*, Nature Nanotechnology **1**, 53 (2006).
17. J. P. Cleuziou *et al.*, Phys. Rev. Lett. **99** (2007).
18. A. F. Morpurgo *et al.*, Science **286**, 263 (1999).
19. A. Y. Kasumov *et al.*, Science **284**, 1508 (1999).
20. A. Eichler *et al.*, Phys. Rev. Lett. **99**, 126602 (2007).
21. J. Kong *et al.*, Nature **395**, 878 (1998).

22. M. Octavio *et al.*, Phys. Rev. B **27**, 6739 (1983).
23. M. R. Buitelaar *et al.*, Phys. Rev. Lett. **88**, 156801 (2002).
24. C. W. J. Beenakker and H. van Houten, in *Single Electron Tunneling and Mesoscopic Devices*, edited by H. Koch and H. Lubbig (Springer, Berlin, 1992).
25. M. Tinkham, *Introduction to Superconductivity* (McGraw-Hill Book Co., 1996).
26. C. Zhong, J. Kong, and H. Dai, Phys. Rev. Lett. **84**, 5604 (2000).
27. A. M. Goldman and N. Markovic, in *Physics Today*, 1998, p. 39.

Fig. 1.(a). Normal state conductance of a SWNT device as a function of  $V_g$ . Inset: device schematic. (b). Differential conductance as functions of bias  $V_g$ . (c). same as (b) at small bias. Notice the logarithmic color scale.

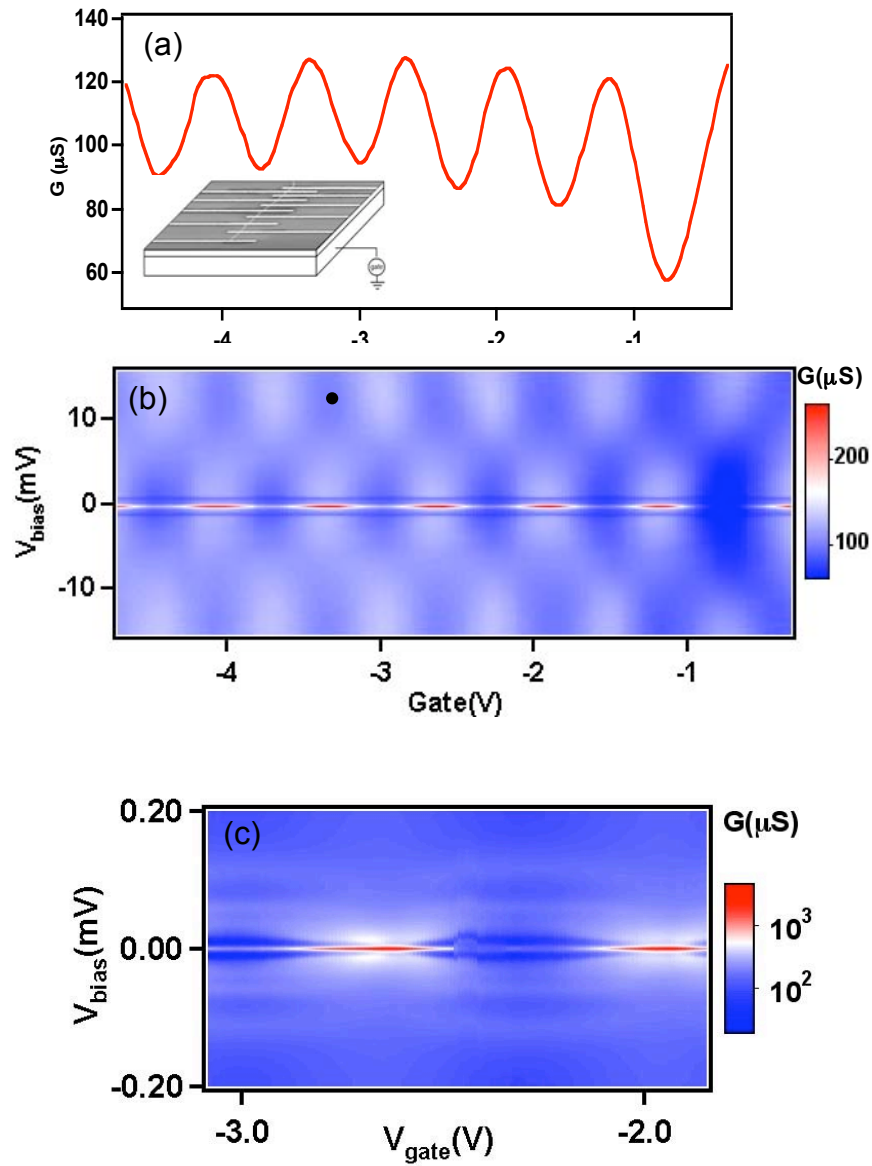


Fig. 2. (a).  $V$ - $I$  characteristics of a S/SWNT/S device at 260mK at 3 different gate voltages. Inset:  $\gamma$  curve at large current bias. (b) Measured voltage across the device as functions of bias current and gate voltage.  $\alpha$ ,  $\beta$  and  $\gamma$  indicates gate voltages at which line traces in (a) are taken.

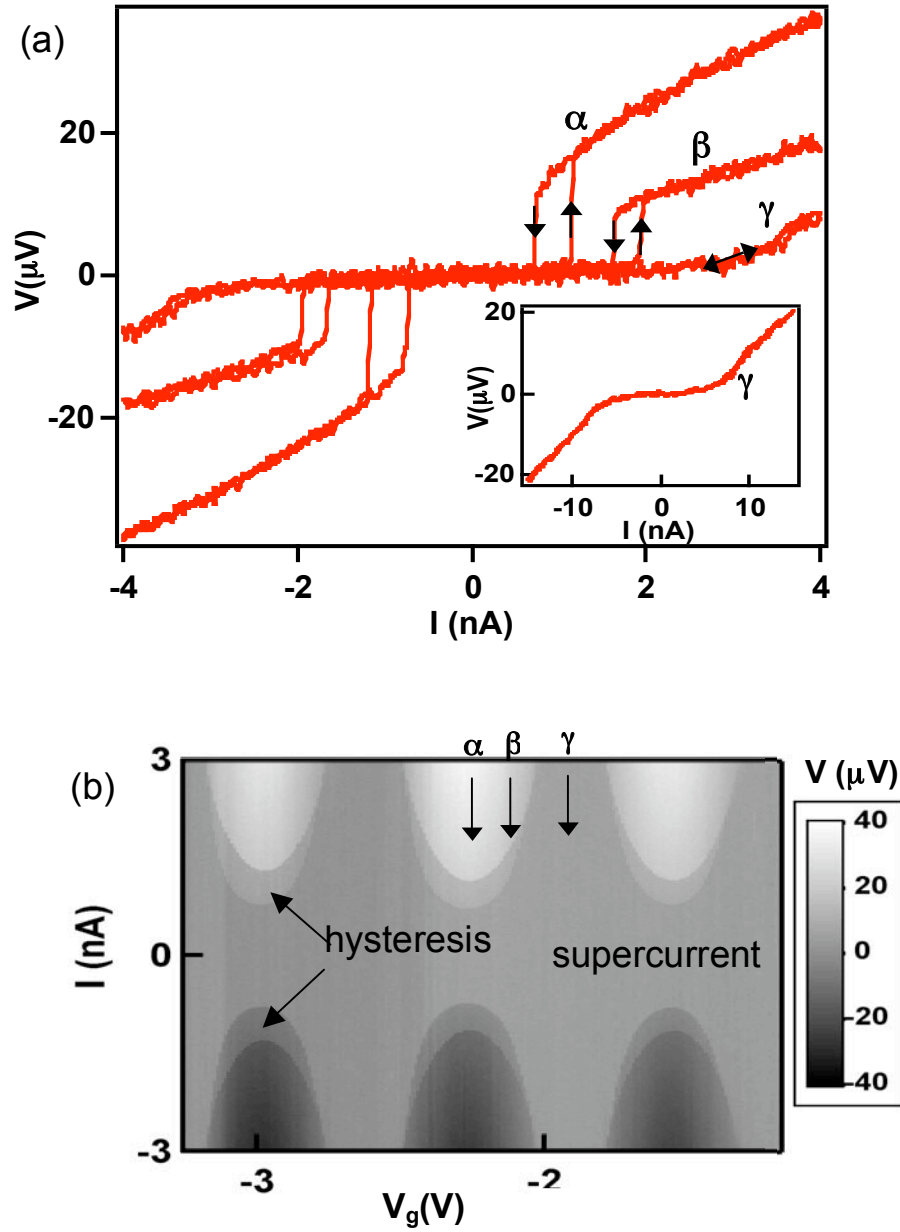


Fig. 3. Upper panel:  $I_c$  (open circles) and  $I_r$  (closed circles) vs.  $V_g$ . Lower Panel:  $I_c/I_r$  (triangles, left axis) and  $G_N$ (dotted line, right axis) vs  $V_g$ .

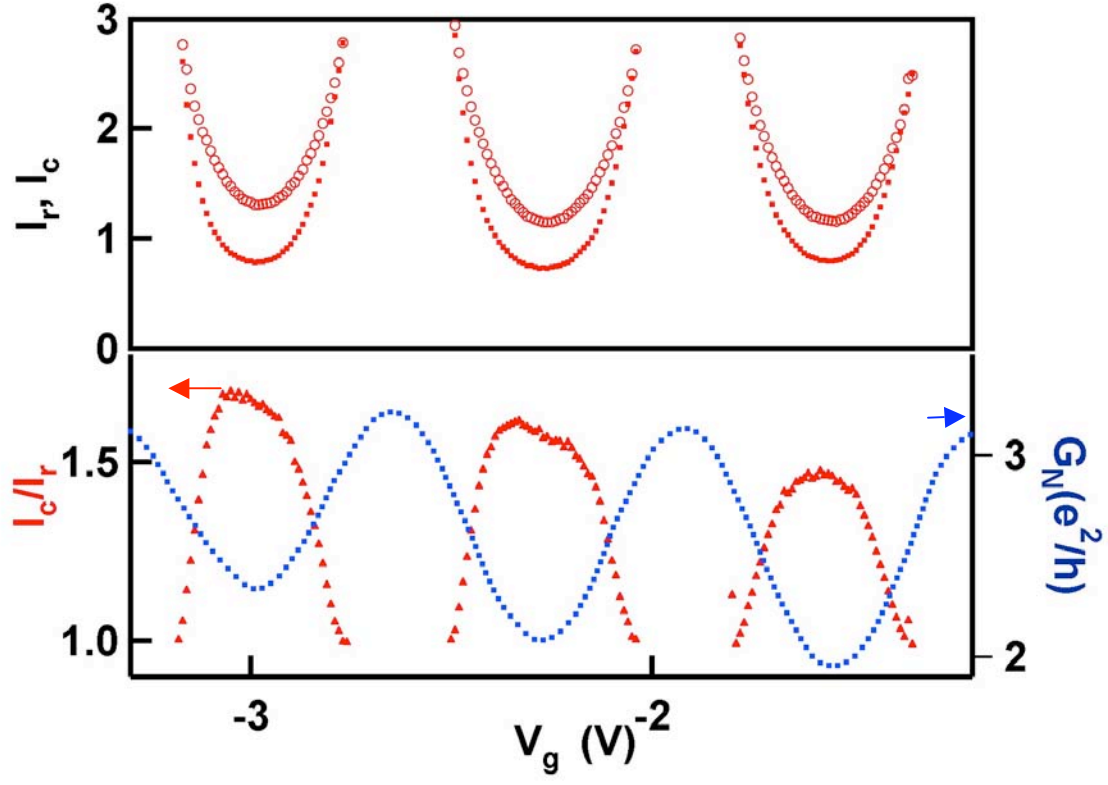


Fig. 4. (a). Upper Inset:  $G_N$  vs  $V_g$  for a device with a conductance minimum at  $V_g \sim 10.5$ V. Main Panel:  $V$ - $I$  characteristics at  $V_g=10.5$ V at  $T=0.7$ K (red),  $0.5$ K (green) and  $0.26$ K (blue). Lower Inset: same as main panel with larger bias range. Middle Inset:  $V$ - $I$  curves outside the gap at  $T=0.9$ K (red),  $0.53$ K (green) and  $0.26$ K (blue).

(b). Resistance vs  $T$  at different  $V_g$ . The top curve corresponds to that at  $V_g=10.5$ V.

